*Pharmaceutical Research, Vol. 23, No. 11, November 2006 (© 2006)*
DOI: 10.1007/s11095-006-9137-8

*Featured Article*

# PAMPA–Excipient Classification Gradient Map

**Stefanie Bendels,[1] Oksana Tsinman,[2] Björn Wagner,[1] Dana Lipp,[2] Isabelle Parrilla,[1] Manfred Kansy,[1] and Alex Avdeef [2,3]**

*Received April 14, 2006; accepted July 27, 2006; published online October 20, 2006*

***Abstract.*** The effect of excipients on the artificial membrane permeability (Double-Sink PAMPA) properties of eight sparingly soluble drugs was studied. Quantities of excipient were selected to match the concentrations expected in the gastrointestinal fluid under clinically relevant conditions. Over 1,200 measurements were performed. To correct for the effects of the aqueous boundary layer and determine the intrinsic permeability, precisely measured ionization constants were used. The intrinsic permeability of weak acids was enhanced (up to 100 fold) but that of weak bases depressed (up to 270 fold) by the excipients: mefenamic acid > glybenclamide > progesterone > griseofulvin > clotrimazole > astemizole > dipyridamole > butacaine. Excipient enhancement ranked: 3 mM NaTC > 0.24% PEG400 > 0.2 M KCl > 0.24% NMP > 5% PEG400 > 0.24% PG > 1% PEG400 > 0.1M KCl > 1% PG > 1% NMP > 5% PG > 0.24% HP-β-CD > 1% HP-β-CD > 15 mM NaTC. The study clearly indicates that the method is suitable for use in preclinical development to assess the effect of excipients on the permeability of sparingly soluble drug candidates. The method is quick, cost-effective, and reasonably accurate. The self-rank-ordered PAMPA-Mapping may be a helpful visualization tool for delivery screening.

**KEY WORDS:** Double-Sink PAMPA; excipients; flux p$K_a$; HP-β-CD; PAMPA-Mapping; PEG400; propylene glycol; sodium taurocholate; 1-methyl-2-pyrrolidone.

## INTRODUCTION

Orally delivered drugs must cross the gastrointestinal barrier, if they are to reach their systemic therapeutic target sites. The rate and extent of entry of a drug from the gastrointestinal luminal fluid into the blood stream depends on many physicochemical factors, including lipophilicity, molecular size and flexibility, charge state, and hydrogen-bonding potential (both H-bond count and three-dimensional distribution within the molecule) (1–3). Large, polar or ionized molecules are usually poorly absorbed because of low permeability across the gastrointestinal tract (GIT) barrier. This is a problem difficult to overcome by formulation strategies (4,5). However, molecules with high intrinsic permeability can also be poorly absorbed, if their aqueous solubility is extremely low. Combinatorial chemistry programs often tend to select for such molecules (4,5). Solubilizing excipients can overcome some of the poor absorption. But this is not usually considered in discovery. Generally, delivery strategies incorporating excipients are explored in early development, to overcome the poor absorption of the latter class of molecules (6,7).

In discovery, cultured monolayer cell models, such as Caco-2 or MDCK (8,9), are often used to screen for permeability, but by the time the selected candidate molecules are passed into the development phase, such cellular studies are not usually used to select excipients. Commonly, pharmacokinetic animal models are used at that stage.

In the case of sparingly soluble, but otherwise promising molecules, early excipient screening, perhaps as a first step in early preclinical development, would be beneficial in prioritizing and perhaps minimizing the number of animal measurements, if a cost effective means were available to measure the effect of excipients on permeability. Liu *et al.* (10) were the first to propose to do just that, using the low-cost PAMPA (parallel artificial membrane permeability assay) model specifically for screening the solubilizing agents Brij® 35, Cremophor EL, ethanol, and Tween 80. Up to that time, PAMPA had been a useful probe, but solely in early discovery screening (11). Since then, the value of PAMPA as a useful mechanistic tool for medicinal chemists has been demonstrated in several instances (12–14), but aside from the work of Liu *et al.,* the impact of PAMPA in early preclinical development had not been substantiated.

In this study, we propose to extend the theme explored by Liu *et al.* We report the Double-Sink PAMPA measurements of eight sparingly soluble drugs: astemizole, butacaine, clotrimazole, dipyridamole, griseofulvin, progesterone, glybenclamide, and mefenemic acid, measured under 15 combinations of six excipients and ionic strength adjusters: sodium

Contribution number 21 in the *PAMPA—a Drug Absorption in vitro Model* series from *p*ION. (14) is part 17 in the series. Double-Sink™, Gut-Box™, and PAMPA-Mapping™ are trademarks of *p*ION INC.

[1] Pharmaceutical Division, F. Hoffmann–La Roche Ltd., PRBD-C, CH-4070, Basel, Switzerland.
[2] pION INC, 5 Constitution Way, Woburn, Massachusetts 01801, USA.
[3] To whom correspondence should be addressed. (e-mail: aavdeef@pion-inc.com)

taurocholate, 2-hydroxypropyl-β-cyclodextrin, potassium chloride, propylene glycol, 1-methyl-2-pyrrolidone, and polyethylene glycol 400, to assess the effect of excipients on permeability. The Double-Sink PAMPA model was selected as a indicator of transport across the GIT barrier. The latter model was originally formulated to match human jejunal permeability measurements, as described elsewhere (3). The original PAMPA study (11) addressed the semiquantitative prediction of human intestinal absorption, and the application of the Double-Sink model to that end has been recently reviewed (14). Our aim here was to develop a practical and cost-effective high-throughput assay, which could be used in early screening for passive intestinal permeability under GIT-relevant conditions of excipients.

## MATERIALS AND METHODS

### Drugs and Chemicals

The compounds used in this study, listed in Table I, were purchased from Sigma-Aldrich (St. Louis, MO, USA). The Double-Sink PAMPA lipid was obtained from *p*ION (PN 1100669), and was stored at −20°C when not used. The pH of the assayed donor solutions was adjusted with universal buffers (*p*ION, PN 100621, 1100151), and the buffer solution at pH 7.4 containing a chemical scavenger to simulate serum proteins (*p*ION ASB-7.4 buffer, PN 110139) was used as the receiver solution. Excipients were purchased from Sigma-Aldrich (St. Louis, MO, USA) except polyethylene glycol 400 (PEG 400), which was purchased from EM Science (VWR). Excipients were added only to the donor wells.

### Excipient Concentrations

Quantities of the six excipients were selected to overlap the concentrations expected in the gastrointestinal fluid under clinically relevant conditions. For KCl, two levels were selected: 0.1 and 0.2 M, according to their concentration in FASSIF/FESSIF media (15). Sodium taurocholate (NaTC) solutions were prepared at 3 and 15 mM, corresponding to fasted and fed GIT states (15). For liquid excipients, the maximum capsule volume was assumed to be 0.6 ml: for a GIT volume of 250 ml (15), the calculated excipient concentration is 0.24% v/v. Hence, for 1-methyl-2-pyrrolidone (NMP), propylene glycol (PG), and polyethylene glycol 400 (PEG400), excipient solutions of 0.24, 1, 5% v/v were tested. 2-Hydroxypropyl-β-cyclodextrin (HP-β-CD) solutions were tested in a similar concentration of 0.24 and 1% w/v. In all, counting the excipient-free buffer solutions, 15 different solutions were tested with the eight drug molecules for the effect on PAMPA, resulting in 120 drug-excipient combinations.

### p$K_a$ Measurement

The potentiometric Gemini (*p*ION), GLpKa (Sirius Analytical Instruments, UK), and UV-metric D-PAS (Sirius), and SGA (Sirius) instruments were used to determine precision ionization constants. With these sparingly soluble compounds, several strategies were tried to overcome experimental difficulties, including the use of DMSO and methanol as cosolvents. In the Gemini instrument, it is possible to determine the p$K_a$ even if there is precipitation during a portion of the titration, in either aqueous or cosolvent solutions. This is because the instrument can determine solubility and ionization constants simultaneously in the same titration (16–18). Furthermore, pH electrode calibration can be performed "*in situ*" by the Gemini instrument, concurrently with the p$K_a$ determination. This is especially an important feature for determinations in cosolvent solutions when the p$K_a$ is outside of the 4–9 range. This is a substantial improvement in comparison to the traditional procedure of first doing a "blank" titration to determine the four Avdeef–Bucher pH electrode parameters (19).

### PAMPA Method

#### *Data Collection*

The PAMPA Evolution instrument from *p*ION INC (Woburn, MA, USA) was used in this study, with data collected at room temperature (25 ± 2°C). The PAMPA 96-well "sandwich" was preloaded with 96 magnetic stirrers (*p*ION, PN 110212). The typical sample concentrations were about 50 μM in the excipient-containing buffer solutions. The residual DMSO in these solutions was 0.5% v/v. The effective permeability, $P_e$, of each compound was measured in the pH 3 to 10 domain. The donor solutions were varied in pH (NaOH-treated universal buffer), while the receiver solutions had the same pH 7.4 ("gradient-pH sink"). Optimized pH-gradient conditions were selected, using the *p*OD procedure (20), to ensure that the pH values would be above and below

**Table I.** Ionization Constants of the Compounds Studied[a]

| Compound | p$K_a$ 25°C, 0.15 M KCl | Percent Weight $CH_3OH$ | Slope | GOF | Number |
|---|---|---|---|---|---|
| Astemizole | 5.99 ± 0.06 | 40 – 61 | −0.012 | 2.2 | 6 |
| | 8.60 ± 0.04 | 40 – 61 | −0.013 | 1.6 | 6 |
| Butacaine | 2.20 ± 0.11 | 16 – 57 | −0.008 | 1.4 | 6 |
| | 10.09 ± 0.10 | 16 – 57 | −0.021 | 5.4 | 6 |
| Clotrimazole | 6.02 ± 0.05 | 11 – 49 | −0.020 | 3.6 | 6 |
| Dipyridamole | 6.22 ± 0.15 | 5 – 43 | −0.016 | 3.3 | 6 |
| Glybenclamide | 5.75 ± 0.15 | 35 – 75 | 0.008 | 3.0 | 7 |
| Mefenamic acid | 4.39 ± 0.09 | 44 – 74 | 0.018 | 1.7 | 8 |

[a] GOF = Goodness-of-fit (3). The slope parameter comes from the regression of apparent p$K_a$ *vs.* weight percent cosolvent, and usually is negative for bases and positive for acids (25). The number of separate titrations used in the cosolvent method is indicated by *n*.

the $pK_a^{flux}$ value (defined below) of the compounds. The pH variation was necessary in order to correct the effective permeability values for ionization and aqueous boundary layer (ABL) effects (3,9,21). The receiver solutions contained a surfactant mixture ("lipophilic sink") to mimic some of the function of drug-binding proteins (22). Vigorous stirring was employed in the assay, with stirring speed set to produce an ABL thickness about 40 μm (25 μm for progesterone), to match the ABL contribution of the measured permeability to that expected in the GIT (21). The PAMPA sandwich was assembled and allowed to incubate for 30 min for the highly permeable molecules, in a controlled-environment chamber (Gut-Box™, *p*ION PN 110205) with a built-in magnetic stirring mechanism. The sandwich was then separated, and both the donor and receiver wells were assayed for the amount of material present, by comparison with the UV spectrum (230 to 500 nm) obtained from reference standard solutions. Mass balance was used to determine the amount of material remaining in the membrane filter (%*R*) and attached to the plastic walls of the microtitre plate (3).

The effective permeability ($P_e$) was calculated as described previously (3), except that the usable filter area, 0.3 $cm^2$, was multiplied by the apparent porosity, 0.76. This latter step ensures that the ABL thickness determined from PAMPA assays using filters with a different porosity would be on an absolute scale (23).

### *Correcting PAMPA Permeability for the ABL and Charge Effects by the $pK_a^{flux}$ Method*

In the GIT epithelial environment, the ABL thickness is expected to be 30–100 μm, whereas in unstirred PAMPA, the ABL thickness can be as high as 4,000 μm (9,21). By taking PAMPA (stirred or unstirred) data over a range of pH, it is possible to match the effect of the ABL to that expected for the GIT, by applying the $pK_a^{flux}$ method (3,9), briefly described below.

The effective permeability coefficient, $P_e$, is related to the membrane and ABL permeability coefficients, $P_m$ and $P_{ABL}$, respectively, as

$$\frac{1}{P_e} = \frac{1}{P_{ABL}} + \frac{1}{P_m} \tag{1}$$

For ionizable molecules, the membrane permeability, $P_m$, depends on pH of the bulk aqueous solution. The maximum possible $P_m$ is designated $P_o$, the intrinsic permeability of the uncharged species. For monoprotic weak acids and bases, the relationship between $P_m$ and $P_o$ may be stated in terms of the fraction of the uncharged species, $f_o$, as $P_m = P_o f_o$, that is,

$$\frac{1}{P_m} = \frac{10^{\pm(\mathrm{pH}-\mathrm{p}K_a)} + 1}{P_o} \tag{2}$$

with '+' used for acids, and '−' used for bases. Other cases are described elsewhere (3,20,22). The logarithmic form of Eq. 2 describes a hyperbolic curve (cf., Fig. 3, dashed curves), characterized by a horizontal region (indicating intrinsic permeability) and a diagonal region (slope of ±1). In the bend of such curves (slope one-half), the pH is indicative of the $pK_a$ of the molecule. Combining Eqs. 1 and 2 leads to

$$\frac{1}{P_e} = \frac{1}{P_{ABL}} + \frac{10^{\pm(\mathrm{pH}-\mathrm{p}K_a)} + 1}{P_o} \tag{3}$$

With highly permeable molecules, Eq. 2 cannot be used to determine either the $pK_a$ or $P_o$, because of the attenuative effect of the aqueous boundary layer, as indicated by Eq. 3. Such "ABL-limited" transport is observed when $P_o >> P_{ABL}$. This is generally the case with lipophilic drugs, where the *same* $P_e$ is often measured (about $30 \times 10^{-6}$ cm/s), *regardless of the molecules* (9), indicating a property of water rather than membrane. The logarithmic form of Eq. 3 is also a hyperbolic curve, with an apparent $pK_a$ associated with the pH at half-slope positions (cf., Fig. 3, solid-line curves). For highly permeable molecules it is useful to consider the "flux" ionization constant, $pK_a^{flux}$, which refers to the pH value where the resistance to transport across a permeation barrier is 50% due to the ABL and 50% due to the membrane (3,9,24). The approximate hyperbolic log-log equation (which is reasonably accurate when $P_o$ is at least ten times greater than $P_{ABL}$—see Appendix for exact solution)

$$\log P_e \approx \log P_e^{max} - \log\left(10^{\pm(\mathrm{pH}-\mathrm{p}K_a^{flux})} + 1\right) \tag{4}$$

describes the relationship between the effective permeability and the apparent ionization constant. The maximum possible effective (measured) permeability, $P_e^{max}$, is defined as

$$\log P_e^{max} = \log P_{ABL} - \log(1 + P_{ABL}/P_o) \tag{5}$$

When $P_o >> P_{ABL}$ (highly permeable molecules), $P_e^{max} \approx P_{ABL}$, indicating water-limited rather than membrane-limited diffusion.

## RESULTS AND DISCUSSION

### $pK_a$ Measurements—Comparisons of Methods

Figure 1 shows a comparison of the ionization constants determined by the various "state-of-the-art" approaches used. Since all of the compounds were only sparingly soluble in water, cosolvents were used, and the aqueous values were extrapolated by the Yasuda–Shedlovsky (25) approach in the case of GLpKa and D-PAS instruments, and by linear extrapolation to zero wt.% cosolvent in the case of the

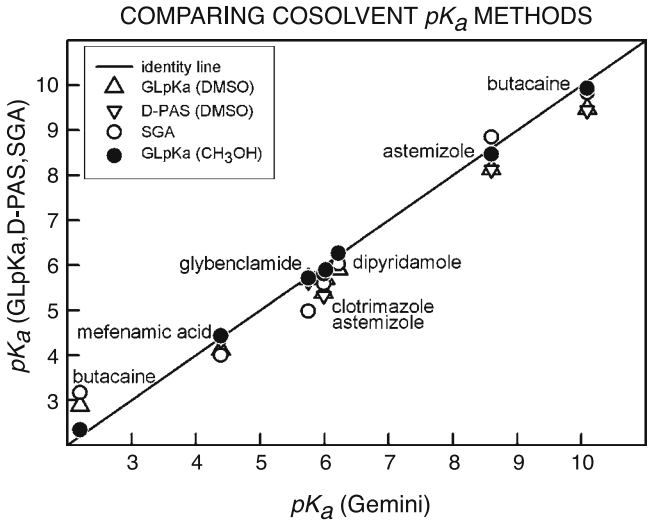


**Fig. 1.** Comparisons of $pK_a$ determination methods.

Gemini instrument. The commercially configured SGA instrument available to us does not have a cosolvent capability, so only aqueous universal buffers were used. Since the D-PAS and SGA instruments are UV-based, it was possible to use lower-concentration solutions in the p$K_a$ determination, avoiding some, *but not all*, of the problems of low aqueous solubility. Two of the most popularly used cosolvents were employed in this study: DMSO and methanol. In just about all of the cases, the DMSO-extrapolated p$K_a$ values were systematically lower than those extrapolated from methanol–water mixtures, following the trend, $pK_a^{DMSO} = 0.61 + 0.86pK_a^{CH3OH} (r^2 = 0.99, s = 0.27, n = 8)$. Since butacaine and astemizole are diprotic bases, it was actually possible to determine the low-pH p$K_a$ in the absence of cosolvent. In both cases, the DMSO-extrapolated values were more biased than those of methanol (cf., Fig. 1). The variance was particularly evident in the case of butacaine low-pH p$K_a$ value. This led us to suspect that the methanol-extrapolated values are more accurate in general, a suspicion supported by methanol being viewed as the "least problematic" of the cosolvents used in p$K_a$ determinations (25). With DMSO results excluded, a decision was made not to rely on the SGA values in this study, since cosolvent use was not an available feature, and since the deviations from the identity line in Fig. 1 were substantial. Figure 1 reveals that best concordance was seen between potentiometric GLpKa and Gemini values, as indicated by the filled circles being closest to the identity line.

The GLpKa and Gemini values could have been simply averaged for the working set. We opted not to do that for two reasons. In spite of well designed assays, where the cosolvent–water ratios are picked to be sufficiently high to avoid precipitation, it is nearly impossible to be certain that precipitation does not occur at the lowest cosolvent–water ratios. In the GLpKa, the solutions cannot be easily observed during the titration; the Gemini instrument allows a clear view of the glass assay vial. Such visual observations suggested that it was highly probable that in a number of cases, some precipitation must have taken place in the GLpKa with these low solubility compounds (The p$K_a$ bias due to precipitation is overcome by the Gemini computational procedure, as indicated below). Secondly, the Gemini *in situ* electrode calibration procedure leads to more reliable p$K_a$ determinations in cosolvent solutions in the pH < 3 domain.

### p$K_a$ Measurements—Gemini Results

Figure 2 illustrates what can conceivably go "wrong" with conventionally designed p$K_a$ assays, and the usual consequences in conventional measurements, which by contrast are circumcalculated by the Gemini. Illustrated in Fig. 2 are six determinations of the clotrimazole p$K_a$ in 11–49 wt.% methanol. The zero-cosolvent extrapolated p$K_a$ is 6.02 ± 0.05.

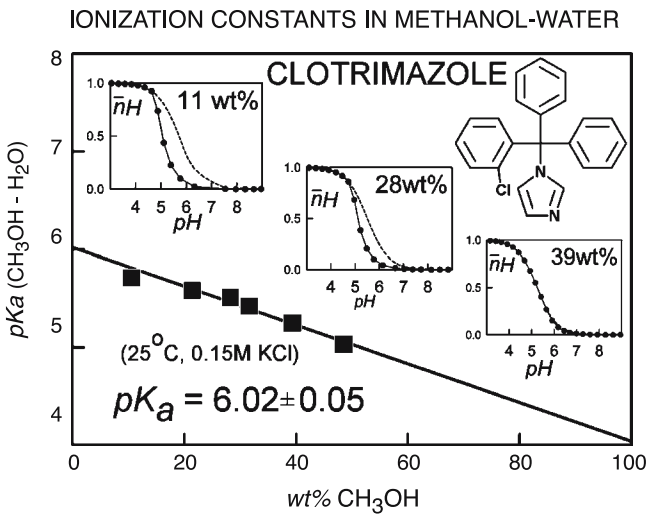


**Fig. 2.** Linear extrapolation of apparent p$K_a$ determined in various mixtures of methanol–water. The fit is weighted by the errors in the ionization constants determined by the Gemini software. The *insets* are Bjerrum plots indication precipitation during some of the titrations (see text).

The insets in Fig. 2 are Bjerrum plots (3,16,26) for the 11, 28, and 39 wt.% titrations (The pH at the half-integral position in the Bjerrum function is equal to the p$K_a$). The dashed curves in the insets correspond to the expected curves in the limit of infinitely low concentration of sample, where no precipitation would take place. The solid curves, linking the measured points indicate a significant displacement from the precipitation-free dashed curves. This displacement takes place because clotrimazole precipitated in titrations below 35 wt.% methanol. Conventional refinement programs, not taking such precipitation into effect, would have systematically underestimated the p$K_a$ with decreasing cosolvent ratios, with an error as high as a log unit in the case of 11 wt.% (Fig. 2 inset). If the biased values were the basis of extrapolation, the p$K_a$ would have been near 5, a log unit off (data not shown).

The unique aspect of the refinement program in the Gemini instrument is that it can determine the unbiased p$K_a$ value in the presence of some precipitation, since the solubility and the p$K_a$ values are simultaneously refined. This is an extension of the original potentiometric solubility method first described by Avdeef and coworkers (16–18). The fit in Fig. 2 is weighted by the errors obtained in the individual-set refinements, which automatically down-weighs the contributions of the lowest wt.% cosolvent points, if "too much" precipitation prevents a precise determination of the p$K_a$ value.

The novel p$K_a$ technology is best suited for determining the ionization constants of the most insoluble compounds. The following improvements are evident: (a) a wider span of cosolvent ratios is feasible, since precipitation at the lower

**Fig. 3.** The log permeability *vs.* pH plots of the eight molecules measured by the Double-Sink PAMPA method. The best-fit of Eq. 4 to the measured effective permeability data are represented by the *solid curves*, and the derived log $P_m$ − pH curves, according to Eq. 2, are represented by *dashed curves*. The *dotted lines* correspond to the log $P_{ABL}$ values, derived from the refinement model based on Eq. 4. The maximum point in the log $P_m$ curves corresponds to the intrinsic permeability coefficient, log $P_o$, which characterizes the transport of the neutral form of an ionizable molecule. The intersections of the horizontal and the diagonal tangents occur at pH values corresponding to the p$K_a$ in the *dashed curves* and the $pK_a^{flux}$ in the *solid curves.*

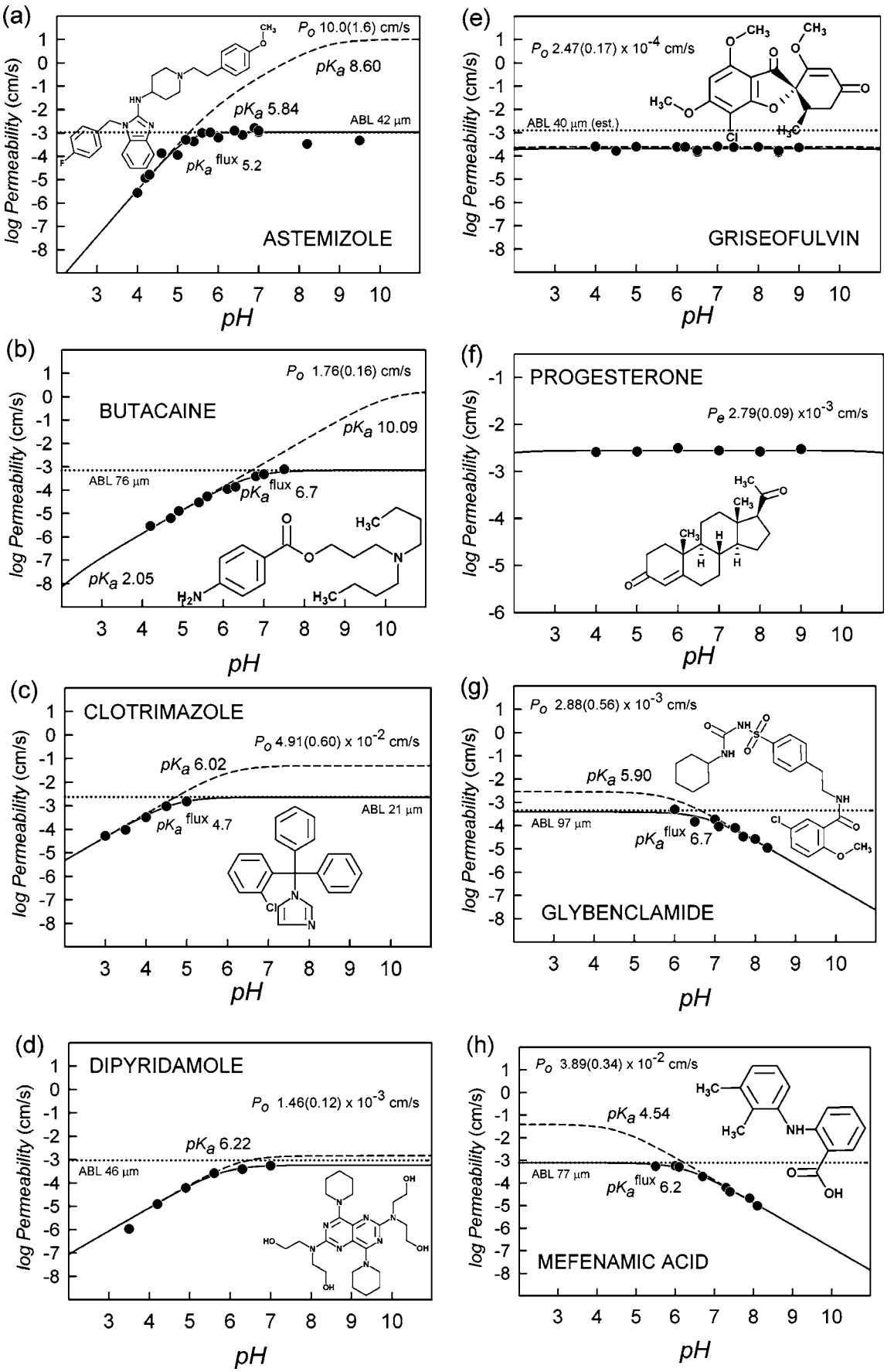
(a)
ASTEMIZOLE
$P_o$ 10.0(1.6) cm/s
$pK_a$ 8.60
$pK_a$ 5.84
ABL 42 μm
$pK_a^{flux}$ 5.2
(b)
BUTACAINE
$P_o$ 1.76(0.16) cm/s
$pK_a$ 10.09
ABL 76 μm
$pK_a^{flux}$ 6.7
$pK_a$ 2.05
(c)
CLOTRIMAZOLE
$P_o$ 4.91(0.60) x $10^{-2}$ cm/s
$pK_a$ 6.02
ABL 21 μm
$pK_a^{flux}$ 4.7
(d)
DIPYRIDAMOLE
$P_o$ 1.46(0.12) x $10^{-3}$ cm/s
$pK_a$ 6.22
ABL 46 μm
(e)
GRISEOFULVIN
$P_o$ 2.47(0.17) x $10^{-4}$ cm/s
ABL 40 μm (est.)
(f)
PROGESTERONE
$P_e$ 2.79(0.09) x$10^{-3}$ cm/s
(g)
GLYBENCLAMIDE
$P_o$ 2.88(0.56) x $10^{-3}$ cm/s
$pK_a$ 5.90
ABL 97 μm
$pK_a^{flux}$ 6.7
(h)
MEFENAMIC ACID
$P_o$ 3.89(0.34) x $10^{-2}$ cm/s
$pK_a$ 4.54
ABL 77 μm
$pK_a^{flux}$ 6.2
log Permeability (cm/s)
pH

ratios is circumcalculated, (b) higher concentrations of sample may be used, for more sensitive determination, (c) selecting the "best" cosolvent ratios is less critical to the extrapolation process, making the method more "fault" tolerant, and (d) *in situ* pH electrode calibration makes p$K_a$ determinations in a wider pH window more accurate in cosolvent titrations.

Table I lists the Gemini-determined p$K_a$ values at 0.15 M (KCl) ionic strength. These values were subsequently converted to 0.01 M ionic strength level and used in the PAMPA analyses, since the permeability buffer is at the lower ionic strength. In the case of 0.1 and 0.2 M KCl, appropriate adjustments to the constant were made (3).

## PAMPA Measurements without Excipients

Figure 3 shows the excipient-free permeability profiles for the molecules studied. Solid lines indicate the best fit of the effective permeability values, log $P_e$ (filled circles), as a function of pH, according to Eq. 4. Sample values of p$K_a^{flux}$ are indicated in Fig. 3(a–c,g,h).

The dashed-line membrane permeability curves, log $P_m$ *vs.* pH, result when the calculated aqueous boundary layer (ABL) permeability values (dotted horizontal lines) are factored out of the effective permeability values (Eqs. 1 and 2). The solid-line curves in Fig. 3 [all, except (d) and (e)] are examples of ABL-limited transport, since at their maximum extent, they are substantially below the dashed-line curves. With bases, for pH $>>$ p$K_a^{flux}$, Eq. 4 is that of a horizontal line, and for pH $<<$ p$K_a^{flux}$, Eq. 4 is that of a diagonal line, with a slope of +1. With acids, for pH $<<$ p$K_a^{flux}$, Eq. 4 is that of a horizontal line, and for pH $>>$ p$K_a^{flux}$, Eq. 4 is that of a diagonal line, with a slope of −1.

Since the direct p$K_a^{flux}$ method cannot be used with nonionizable molecules (griseofulvin and progesterone), an indirect calibration procedure was used (9,21). The refined ABL thicknesses (Eq. 4) are indicated in Fig. 3, and range from 21–97 μm. The three values exceeding 75 μm may indicate that butacaine, mefenamic acid, and glybenclamide are aggregated in excipient-free buffer solution. Since ABL permeability depends on molecular weight of the species diffusing in aqueous solution, the use of the monomer molecular weight in calculations leads to an increased *apparent* ABL thickness (9,21).

## PAMPA Measurements with Excipients

Over 1,200 Double-Sink PAMPA measurements were performed in the pH range 3–10. In this study, permeability–pH measurements were used to determine the pH-independent intrinsic value. This is the transport property of the molecule, apart from the environmental factor influences, such as the pH and ABL effects. It was particularly of interest to determine how excipients affect this molecular transport property. To calculate precise intrinsic permeability, high-precision p$K_a$s (Gemini) were used for the p$K_a^{flux}$ method. Table II compiles the 120 $P_o$ values determined in this study, along with the maximum membrane retention (%R), and apparent ABL thicknesses (μm).

The most permeable molecule is astemizole, with $P_o$ values ranging from 0.5 (0.24% v/v PEG400 and 15 mM NaTC) to 32 cm/s (3 mM NaTC). The least permeable molecule is griseofulvin, with $P_o$ values ranging from $1.8 \times 10^{-4}$ (5% v/v PG) to $4.1 \times 10^{-4}$ cm/s (0.1 M KCl).

Membrane retention was substantial in most molecules, with astemizole ranking the highest, with values in the range 79–90% typically (but dropping to 24% in the case of 15 mM NaTC). In spite of such compound depletions from the aqueous phases, it was still possible to access permeability of astemizole by the PAMPA Evolution instrument software. As indicated in Table II, the other retained molecules change in ranking with the excipients. Low membrane retentions indicate that the excipient competes effectively with the PAMPA membrane in holding on to the compounds, as for example in the case of 15 mM NaTC, particularly for clotrimazole, where retention drops to 4%, compared to the excipient-free value of 80%.

The ABL thicknesses listed in Table II are also indicative of excipient–drug interactions. Ideally, if a drug were to form neither aggregates in excipient-free solutions, nor associated complexes with excipients, then the determined ABL thicknesses, $h_{ABL}$, should have been about 40 μm (or 25 μm in the case of the highly stirred progesterone solutions). Indeed, in a number of cases, such as with astemizole and clotrimazole, the expected $h_{ABL} < 50$ μm were determined. However, in stark contrast, the calculated ABL thicknesses in 15 mM NaTC solutions are over 1,000 μm in a number of cases. Table III lists the theoretically expected and the experimental $P_{ABL}$. The lowered observed values could be interpreted to arise from the effect of associated complexes which have very high molecular weights. The relationship between $P_{ABL}$ and MW has been discussed in recent literature (9,14). For example, if Eq. 4 from (14) is applied to the apparent $P_{ABL}$, the excipient-free solutions (0% NaTC, Table III) appear to indicate aqueous diffusion of monomers in the case of astemizole, clotrimazole, and dipyridamole, since the ratio of the apparent molecular weight, MW*(based on the assumption of 40 μm ABL) to the true molecular weight, MW*/MW, is close to 1. In the same buffer solutions, aggregates of the order of 4–7 seem to be indicated for some of the other low-solubility drugs (27). In 3 mM sodium taurocholate solutions, only dipyridamole appears to behave as a monomer (Table III), with the other molecules appearing as aggregates of order 3–5. These "aggregates" can be associations between drug and excipient. In 15 mM NaTC solutions, the reduction in the ABL permeability is extreme, and simplistic analysis indicated aggregation orders as high as 56,000, which does not seem reasonable. It is difficult to be very certain that complexation with the excipient is the only explanation, since 15 mM NaTC solutions are hard to work with in the robotic instrument, due to the occasional slight foaming in the microtitre plate fluidic transfers. The possibility that 15 mM NaTC solution is dissolving some of the PAMPA membrane is of concern, but no visual evidence of the effect (turbidity in solution) was observed. This is being further investigated in our labs.

Figure 4 plots the differences between log $P_o$ in excipient-containing solutions and those of excipient-free (reference level) solutions, as a function of the amount of excipient. In many cases, it is evident that bases behave

**Table II.** Intrinsic Permeability, Maximum Membrane Retention, and Aqueous Boundary Layer Thickness, as a Function of Excipients

| Compound | No excipient | KCl | | NaTC | | HP-b-CD | | NMP | | PG | | | PEG400 | | |
|---|---|---|---|---|---|---|---|---|---|---|---|---|---|---|---|
| | | 0.1 M | 0.2 M | 3 mM | 15 mM | 0.24% | 1% | 0.24% | 1% | 0.24% | 1% | 5% | 0.24% | 1% | 5% |
| Intrinsic permeability (cm/s) | | | | | | | | | | | | | | | |
| Astemizole | 1.0E + 01 | 5.9E + 00 | 1.0E + 01 | 3.2E + 01 | 5.3E − 01 | 1.8E + 01 | 7.9E + 00 | 1.2E + 01 | 6.6E + 00 | 1.9E + 01 | 1.1E + 01 | 1.2E + 01 | 5.4E − 01 | 3.5E + 00 | 4.1E + 00 |
| Butacaine | 1.8E + 00 | 9.0E − 01 | 7.9E − 01 | 2.7E + 00 | 2.5E + 00 | 1.0E + 00 | 4.5E − 01 | 1.1E + 00 | 7.0E − 01 | 2.1E + 00 | 1.5E + 00 | 6.9E − 01 | 1.9E − 01 | 3.7E − 01 | 3.6E − 01 |
| Clotrimazole | 4.9E − 02 | 5.7E − 02 | 4.6E − 02 | 8.9E − 02 | 4.4E − 03 | 3.8E − 02 | 2.6E − 02 | 5.3E − 02 | 4.9E − 02 | 6.9E − 02 | 4.9E − 02 | 4.2E − 02 | 4.8E − 02 | 4.8E − 02 | 4.5E − 02 |
| Dipyridamole | 1.5E − 03 | 7.0E − 04 | 9.8E − 04 | 1.5E − 03 | 4.1E − 04 | 1.7E − 03 | 1.0E − 03 | 1.1E − 03 | 1.1E − 03 | 1.8E − 03 | 1.5E − 03 | 6.1E − 04 | 4.7E − 04 | 4.1E − 04 | 5.6E − 04 |
| Griseofulvin | 2.5E − 04 | 4.1E − 04 | 3.3E − 04 | 3.2E − 04 | 2.1E − 04 | 3.0E − 04 | 3.7E − 04 | 3.3E − 04 | 2.5E − 04 | 2.9E − 04 | 2.7E − 04 | 1.8E − 04 | 2.6E − 04 | 3.7E − 04 | 2.0E − 04 |
| Progesterone | 2.8E − 03 | 5.3E − 03 | 4.7E − 02 | 2.8E − 01 | 1.0E − 05 | 4.3E − 04 | 1.1E − 04 | 1.9E − 02 | 8.1E − 03 | 4.8E − 03 | 5.3E − 03 | 8.3E − 03 | 8.4E − 03 | 8.9E − 03 | 1.6E − 02 |
| Glybenclamide | 2.9E − 03 | 3.5E − 03 | 6.1E − 03 | 8.2E − 04 | 5.5E − 03 | 2.1E − 03 | 8.5E − 04 | 8.8E − 03 | 5.4E − 03 | 2.3E − 03 | 2.6E − 03 | 1.1E − 03 | 3.0E − 01 | 2.0E − 02 | 2.1E − 02 |
| Mefenamic acid | 3.9E − 02 | 1.1E − 01 | 1.2E − 01 | 3.7E − 02 | 7.1E − 02 | 2.1E − 02 | 7.4E − 03 | 6.2E − 02 | 4.8E − 02 | 4.2E − 02 | 3.6E − 02 | 3.3E − 02 | 3.4E + 00 | 3.3E − 01 | 3.3E − 01 |
| Maximum membrane retention (%$R$) | | | | | | | | | | | | | | | |
| Astemizole | 84 | 87 | 89 | 84 | 24 | 83 | 84 | 82 | 79 | 88 | 87 | 90 | 82 | 85 | 86 |
| Butacaine | 57 | 63 | 61 | 41 | 47 | 51 | 50 | 48 | 50 | 58 | 64 | 70 | 29 | 56 | 42 |
| Clotrimazole | 74 | 66 | 63 | 34 | 4 | 61 | 60 | 60 | 53 | 63 | 72 | 80 | 58 | 69 | 57 |
| Dipyridamole | 74 | 76 | 79 | 54 | 62 | 61 | 57 | 61 | 59 | 73 | 83 | 76 | 55 | 74 | 57 |
| Glybenclamide | 51 | 67 | 67 | 46 | 83 | 64 | 56 | 68 | 62 | 65 | 61 | 74 | 55 | 68 | 67 |
| Mefenamic acid | 74 | 70 | 76 | 56 | 82 | 74 | 59 | 77 | 71 | 75 | 76 | 72 | 64 | 75 | 76 |
| Griseofulvin | 51 | 50 | 43 | 40 | 69 | 45 | 44 | 50 | 46 | 45 | 48 | 41 | 43 | 45 | 42 |
| Progesterone | 70 | 71 | 65 | 55 | 18 | 44 | 34 | 63 | 57 | 62 | 59 | 62 | 58 | 50 | 61 |
| Aqueous boundary layer thickness (μm) | | | | | | | | | | | | | | | |
| Astemizole | 42 | 40 | 52 | 81 | 5,360 | 47 | 47 | 45 | 41 | 36 | 48 | 60 | 65 | 50 | 96 |
| Butacaine | 76 | 124 | 64 | 57 | 4,071 | 86 | 120 | 91 | 79 | 59 | 81 | 71 | 496 | 158 | 501 |
| Clotrimazole | 21 | 43 | 25 | 85 | 1,462 | 34 | 58 | 38 | 29 | 43 | 36 | 47 | 60 | 54 | 58 |
| Dipyridamole | 46 | 17 | 10 | 47 | 918 | 47 | 98 | 48 | 59 | 51 | 62 | 107 | 21 | 27 | 153 |
| Glybenclamide | 97 | 50 | 52 | 56 | 3,644 | 58 | 100 | 57 | 28 | 36 | 73 | 76 | 72 | 64 | 71 |
| Mefenamic acid | 77 | 67 | 91 | 67 | 76 | 72 | 165 | 90 | 89 | 65 | 111 | 159 | 53 | 89 | 101 |

**Table III.** PAMPA Aqueous Boundary Layer Permeability, $P_{ABL}$ ($10^{-6}$ cm/s), In Sodium Taurocholate Solutions

| | | $P_{ABL}$ ($10^{-6}$ cm/s) | | | | MW* / MW[b] | | |
|---|---|---|---|---|---|---|---|---|
| Compound | MW | Theory[a] | 0 mM NaTC | 3 mM NaTC | 3 mM NaTC | 0 mM NaTC | 3 mM NaTC | 15 mM NaTC |
| Astemizole | 458.6 | 1,135 | 1,080 | 561 | 9 | 1 | 5 | 56,000 |
| Butacaine | 306.4 | 1,360 | 713 | 954 | 13 | 4 | 2 | 30,000 |
| Clotrimazole | 344.8 | 1,290 | 2,400 | 604 | –[c] | <1 | 5 | –[c] |
| Dipyridamole | 504.6 | 1,088 | 941 | 922 | 47 | 1 | 1 | 1,100 |
| Glybenclamide | 494.0 | 1,098 | 451 | –[c] | 12 | 7 | –[c] | 24,000 |
| Mefenamic acid | 241.3 | 1,514 | 782 | 909 | 795 | 4 | 3 | 4 |

[a] $P_{ABL}$ calculated from Eq. 4 from (14), assuming molecular weight of non-aggregated drug (monomer) and $h_{ABL} = 40$ μm. [b] Ratio of the calculated apparent molecular weight to that of the non-aggregated drug, calculated from Eq. 4 in (14). [c] Data were not available in the pH region where $P_{ABL}$ can be determined.

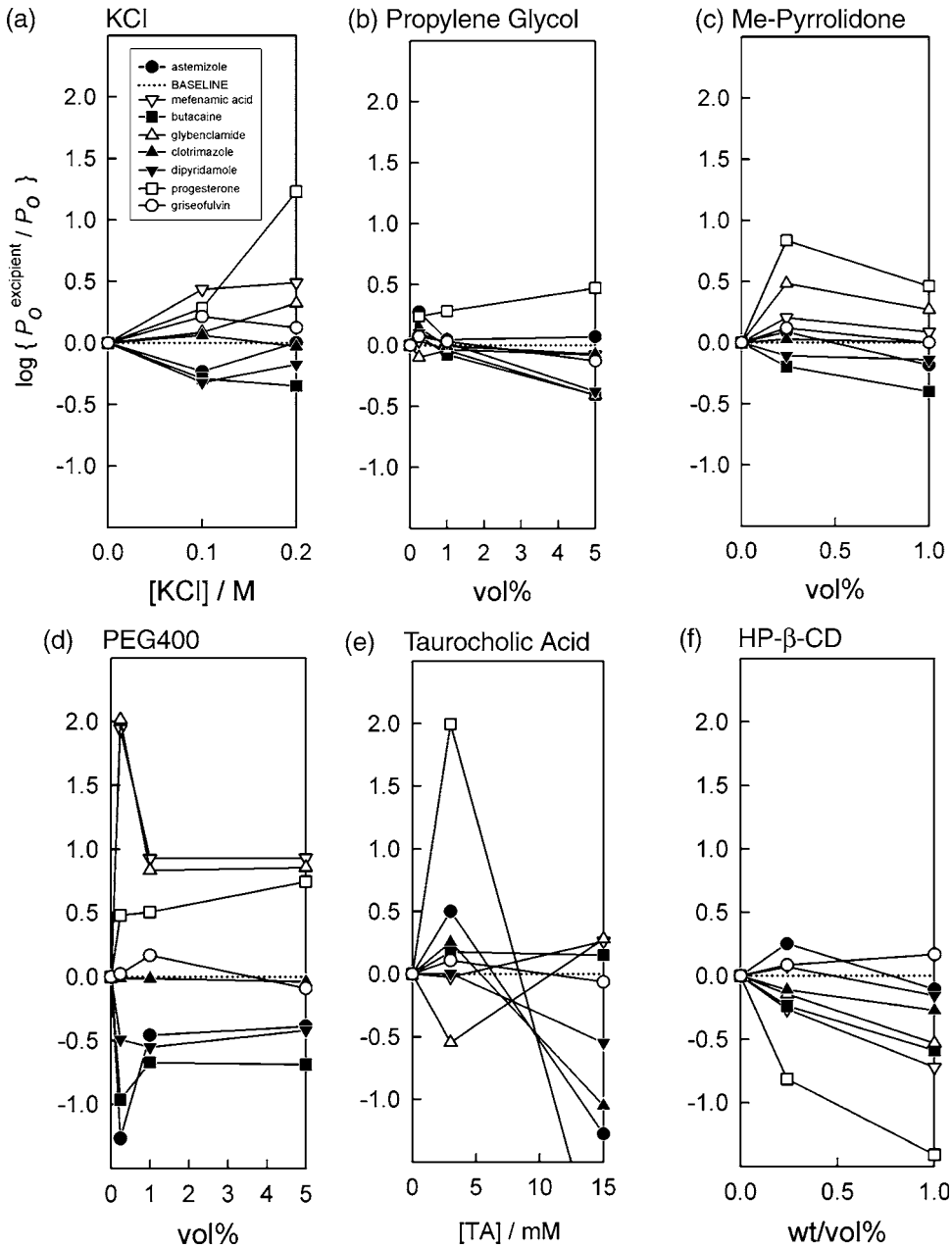


**Fig. 4.** Plot of the difference between log intrinisic permeability in the presence of excipients and the log intrinsic permeability in the absence of excipients, as a function of the quantity of excipient.

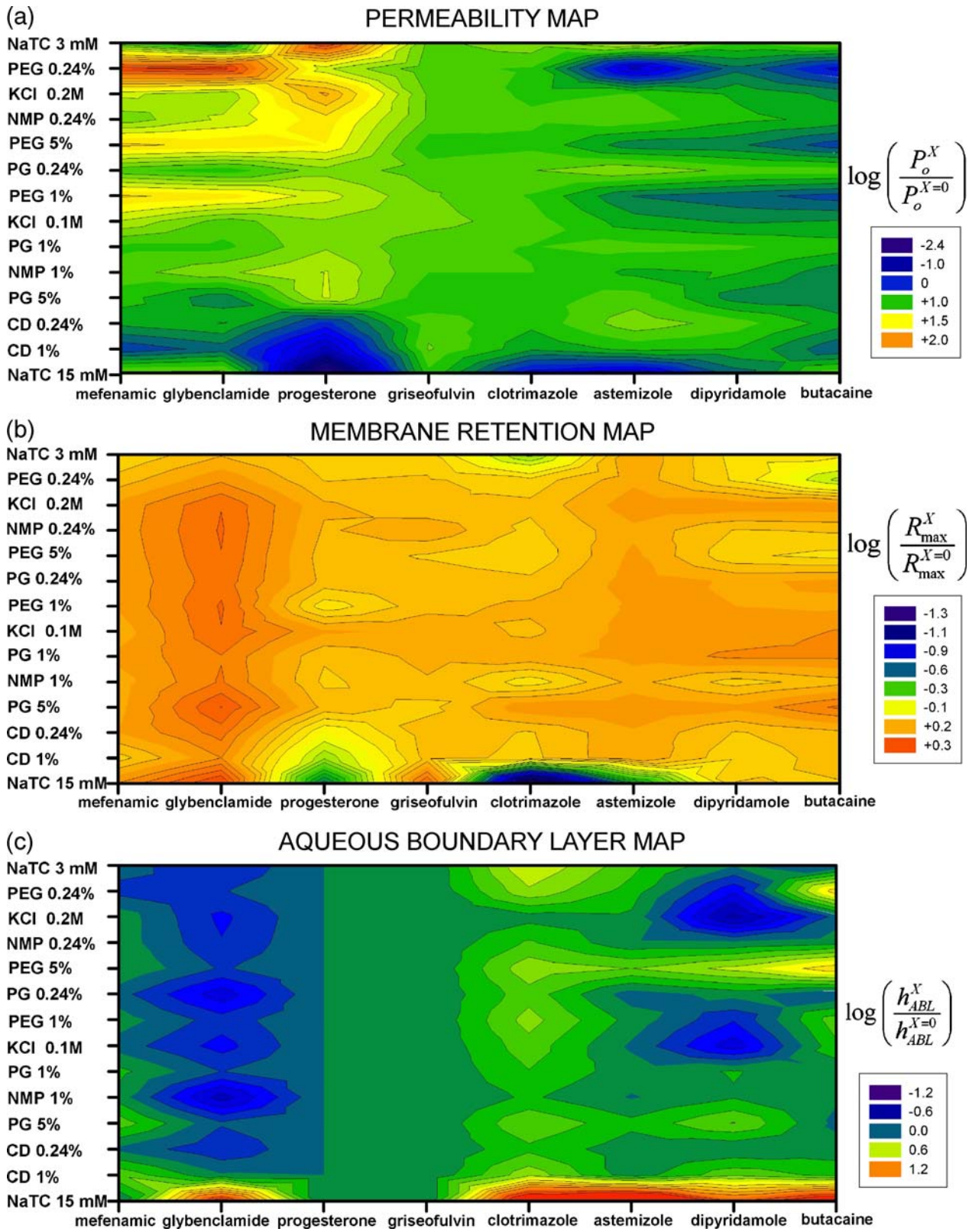


**Fig. 5.** PAMPA-Mapping scheme based on log intrinsic permeability ratio, log membrane retention ratio, and log aqueous boundary layer thickness ratio contour plots, where the vertical axes represent the excipients, rank ordered by decreasing influence of effect *vs.* the compounds arranged in the order of most promising improvements to least promising improvements. The *top left corner* identifies the most promising combinations of excipients and drugs.

differently from acids and neutrals. In KCl, NMP, and PEG400 solutions, bases appear to have lowered intrinsic permeabilities in the presence of excipients, while acids and neutrals have elevated permeabilities. For NaTC and HP-β-CD containing solutions, at the highest level of excipient, all compounds appear to have diminished permeability. Apparently, the binding of drugs to such excipients is sufficiently strong, that the remaining free fraction of the unbound drug concentrations drop significantly, so that the concentration gradient between the donor and acceptor compartments in the permeation cell decreases, leading to decreased flux.

## PAMPA-Mapping

Although Fig. 4 describes the effect of the excipients, it is visually difficult to grasp quickly and use in practical decision making regarding the choice of excipients to enhance drug transport. We propose a mapping scheme shown in Fig. 5, called the PAMPA–Excipient Classification Gradient Map, or simply "PAMPA-Mapping," which improves the visual aspects of the excipient effects. Shown are three component maps of PAMPA-Mapping: permeability, membrane retention, and aqueous boundary layer. Along the vertical axes are the excipient compositions, automatically rank ordered by their enhancement effect on intrinsic permeability. Along the horizontal axes are the drugs, automatically arranged in the order of most enhanced to least enhanced permeability. On the average across all excipients, the intrinsic permeability of acids and neutrals is enhanced, but depressed for the bases. The warm colors indicate an increase in the property mapped as a result of an excipient, where the reference level is defined by excipient-free result. The cool colors indicate the opposite. For example, if the design objective is to enhance membrane transport, the top left corner of the permeability map identifies the molecules and excipient combinations that are most promising for this, and the bottom right corner of the map reveals regions that are least promising.

The membrane retention map (Fig. 5b) is expected to be redundant to the permeability map (Fig. 5a), since it is a measure of the partitioning behavior of the drug between the aqueous solution and the lipid phase of the PAMPA barrier. If simplistic Fick's law of diffusion were solely predictive of transport, than the two maps should be the same in principle. However, it can be seen that there are subtle differences between them, suggesting a slightly non-Ficksian behavior produced by the membrane barrier. The origin of this difference is not entirely understood. Perhaps the permeant concentration gradients across the membrane barrier are not strictly linear, as would be expected under steady-state conditions in simple isotropic membrane barriers.

The ABL map is roughly a mirror image of the other two maps. The elevated $h_{ABL}$ ratios may be interpreted to mean high drug-excipient interaction, leading to slower diffusion in the aqueous layer and decreased membrane retention. An unanticipated effect observed in the ABL map is that some drugs form aggregates in excipient-free solutions (see above), but in the presence of certain excipients, the tendency for the drugs to self-associate is lessened, if not eliminated. This could be the case with glybenclamide, butacaine and dipyridamole in KCl, 0.24% v/v PG, 1% v/v NMP, and 1% PEG, for example, as indicated by deep-blue regions in the map.

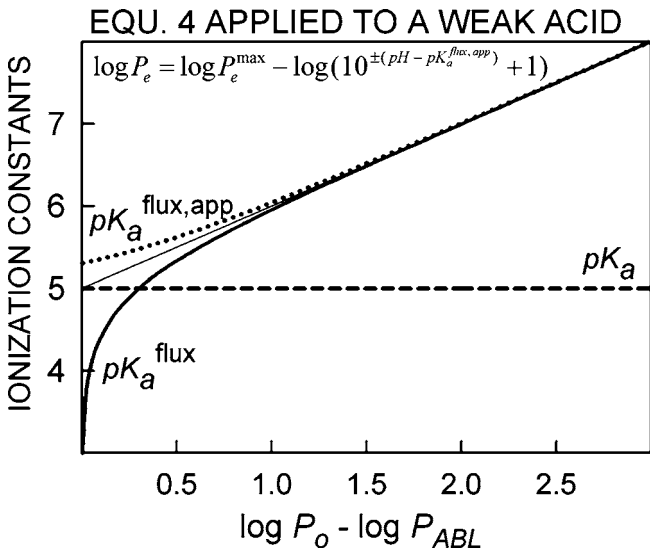


**Fig. 6.** The exact Eq. 4 relationship (applied to a weak acid) between the true p$K_a$ (*dashed curve*), the flux value, p$K_a^{flux}$ (*solid line curve*), and the apparent flux value, p$K_a^{flux,app}$ (*dotted curve*) constants as a function of the difference between the logarithmic intrinsic permeability (log $P_o$) and the aqueous boundary layer permeability (log $P_{ABL}$). The two flux values become nearly equivalent for log $P_o$ − log $P_{ABL} > 1$. The *thin straight line* is the identity line.

## CONCLUSION

We have been able to demonstrate that the Double-Sink PAMPA model can be used to screen for the effect of excipients, and to expand on the earlier observations by Liu *et al.* (10), who used an earlier PAMPA model. Here, excipients were found to lower the apparent permeability of bases and elevate those of acids. The formation of aggregates (butacaine, glybenclamide, mefenamic acid) may be indicated by unexpected increases in the *apparent* thickness of the ABL. In 15 mM sodium taurocholate solutions (above critical micelle concentration), the drug–bile salt binding was extensive, severely diminishing drug membrane transport. Cyclodextrin containing solutions showed a similar, but weaker, effect. We conclude that we have met the objectives of our study: to develop a practical and low-cost high-throughput assay method which could be used in early screening for passive membrane transport in the presence of excipients. The PAMPA–Excipient Classification Gradient Map (PAMPA-Mapping) introduced in this study may prove to be very useful visualization and ranking tool in the future, as large numbers of compounds are screened.

## ACKNOWLEDGMENTS

We thank Torsten Hoffmann (Roche) for encouragement and support of this project. We are especially grateful

to the anonymous reviewer for his astute insights into transport equations.

## APPENDIX

The approximation in Eq. 4 is accurate when $P_o > 10\ P_{ABL}$, but with mildly lipophilic molecules (cf., Fig. 3d—dipyridamole), the exact form is required to calculate $pK_a^{flux}$. The solid-line curve in Fig. 3d only *approximately* indicates the $pK_a^{flux}$ at the pH corresponding to the half-integral slope (that's why no $pK_a^{flux}$ value is noted in Fig. 3d). The precise (more complicated) form of Eq. 4, which can describe the case of dipyridamole is given by

$$\log P_e = \log P_e^{max} - \log\left(10^{\pm(pH - pK_a^{flux,app})} + 1\right) \qquad (6)$$

where *observed* $pK_a^{flux,app}$ is an apparent value, not precisely equal to the true $pK_a^{flux}$. The difference between the two values becomes greater, the smaller the difference between the intrinsic permeability and the ABL permeability. It is tedious, but otherwise straight forward, to derived the explicit logarithmic form of Eq. 3. In the exact solution,

$$pK_a^{flux,app} = pK_a^{flux} \mp \log[(P_o - P_{ABL})/(P_o + P_{ABL})] \qquad (7)$$

where the '−' refers to acids and the '+' sign refers to bases. Figure 6 shows the relationships between the ionization constants as a function of the difference between log $P_o$ and log $P_{ABL}$. Above one log unit of difference (highly lipophilic compounds), $pK_a^{flux,app} \approx pK_a^{flux}$. It should be further emphasized that Eqs. 4 and 6 are only valid when $P_o > P_{ABL}$, as we had noted previously (9,21). In practice, the approximate form (Eq. 3) has proven to be useful in visualizing the balance between membrane and water factors controlling the transport of molecules across biologically relevant membrane barriers.

## REFERENCES


1. H. van de Waterbeemd, D. A. Smith, K. Beaumont, and D. K. Walker. Property-based design: optimization of drug absorption and pharmacokinetics. *J. Med. Chem.* **44**:1313–1333 (2001).
2. H. van de Waterbeemd, D. A. Smith, and B. C. Jones. Lipophilicity in PK design: methyl, ethyl, futile. *J. Comp.-Aided Molec. Des.* **15**:273–286 (2001).
3. A. Avdeef. *Absorption and Drug Development*, Wiley, New York, 2003.
4. C. A. Lipinski. Drug-like properties and the causes of poor solubility and poor permeability. *J. Phamacol. Tox. Methods* **44**:235–249 (2000).
5. C. Lipinski. Poor aqueous solubility—an industry wide problem in drug discovery. *Amer. Pharm. Rev.* **5**:82–85 (2002).
6. J. I. Wells. *Pharmaceutical Preformulation: The Physicochemical Properties of Drug Substances*, Ellis Horwood, Chichester, 1988.
7. A. H. Kibbe. (ed.) *Handbook of Pharmaceutical Excipients*, 5th ed. American Pharmaceutical Association, Washington, District of Columbia, 2005.
8. N. F. H. Ho, T. J. Raub, P. S. Burton, C. L. Barsuhn, A. Adson, K. L. Audus, and R. Borchardt. Quantitative approaches to delineate passive transport mechanisms in cell culture monolayers. In G. L. Amidon, P. I. Lee, E. M. Topp, (eds.), *Transport Processes in Pharmaceutical Systems*. Marcel Dekker, New York, New York, 2000, pp. 219–316.
9. A. Avdeef, P. Artursson, S. Neuhoff, L. Lazorova, J. Gråsjö, and S. Tavelin. Caco-2 permeability of weakly basic drugs predicted with the Double-Sink PAMPA $pK_a^{flux}$ method. *Eur. J. Pharm. Sci.* **24**:333–349 (2005).
10. H. Liu, C. Sabus, G. T. Carter, C. Du, A. Avdeef, and M. Tischler. *In vitro* permeability of poorly aqueous soluble compounds using different solubilizers in the PAMPA assay with liquid chromatography/mass spectrometry detection. *Pharm. Res.* **20**:1820–1826 (2003).
11. M. Kansy, F. Senner, and K. Gubernator. Physicochemical high throughput screening: parallel artificial membrane permeability assay in the description of passive absorption processes. *J. Med. Chem.* **41**:1007–1010 (1998).
12. M. Bermejo, A. Avdeef, A. Ruiz, R. Nalda, J. A. Ruell, O. Tsinman, I. González, C. Fernández, G. Sánchez, T. M. Garrigues, and V. Merino. PAMPA—a drug absorption *in vitro* model. 7. Comparing rat *in situ*, Caco-2, and PAMPA permeability of fluoroquinolones. *Eur. J. Pharm. Sci.***21**:429–441 (2004).
13. M. Kansy, A. Avdeef, and H. Fischer. Advances in screening for membrane permeability: high-resolution PAMPA for medicinal chemists. *Drug Disc. Today: Technologies* **1**:349–355 (2004).
14. A. Avdeef. The rise of PAMPA. *Expert Opin. Drug Metab. Toxicol.* **1**:325–342 (2005).
15. J. B. Dressman. Dissolution testing of immediate-release products and its application to forecasting *in vivo* performance. In J. B. Dressman, and H. Lennernäs, (eds.), *Oral Drug Absorption*, Marcel Dekker, Inc., New York, 2000, pp. 155–181.
16. A. Avdeef. pH–metric solubility. 1. Solubility–pH profiles from Bjerrum plots. Gibbs buffer and $pK_a$ in the solid state. *Pharm. Pharmacol. Commun.* **4**:165–178 (1998).
17. A. Avdeef, C. M. Berger, and C. Brownell. pH–metric solubility. 2. Correlation between the acid–base titration and the saturation shake-flask solubility–pH methods. *Pharm. Res.* **17**:85–89 (2000).
18. A. Avdeef and C. M. Berger. pH–metric solubility. 3. Dissolution titration template method for solubility determination. *Eur. J. Pharm. Sci.* **14**:281–291 (2001).
19. A. Avdeef and J. J. Bucher. Accurate measurements of the concentration of hydrogen ions with a glass electrode: calibrations using the Prideaux and other universal buffer solutions and a computer-controlled automatic titrator. *Anal. Chem.* **50**:2137–2142 (1978).
20. J. A. Ruell, K. L. Tsinman, and A. Avdeef. PAMPA—a drug absorption *in vitro* model. 5. Unstirred water layer in iso-pH mapping assays and $pK_a^{flux}$—optimized design (pOD-PAMPA). *Eur. J. Pharm. Sci.* **20**:393–402 (2003).
21. A. Avdeef, P. Nielsen, and O. Tsinman. PAMPA—a drug absorption *in vitro* model. 11. Matching the *in vivo* aqueous boundary layer by individual-well stirring in microtitre plates. *Eur J. Pharm. Chem.* **22**:365–374 (2004).
22. A. Avdeef. High-throughput measurements of permeability profiles. In H. van de Waterbeemd, H. Lennernäs, and P. Artursson (eds.), *Drug Bioavailability, Estimation of Solubility, Permeability, Absorption and Bioavailability*, Wiley-VCH, Weinheim, 2002, pp. 46–71.
23. P. E. Nielsen and A. Avdeef. PAMPA—a drug absorption *in vitro* model. 8. Apparent filter porosity and the aqueous boundary layer. *Eur. J. Pharm. Sci.* **22**:33–41 (2004).
24. A. Avdeef. Physicochemical profiling (solubility, permeability and charge state). *Curr. Topics Med. Chem.* **1**:277–351 (2001).
25. A. Avdeef, J. E. A. Comer, and S. J. Thomson. pH–metric logP. 3. Glass electrode calibration in methanol–water, applied to $pK_a$ determination of water-insoluble substances. *Anal. Chem.* **65**:42–49 (1993).
26. A. Avdeef, D. L. Kearney, J. A. Brown, and A. R. Chemotti Jr.. Bjerrum plots for the determination of systematic concentration errors in ttitration data. *Anal. Chem.* **54**:2322–2326 (1982).
27. W. H. Streng, D. H.-S. Yu, and C. Zhu. Determination of solution aggregation using solubility, conductivity, calorimetry, and pH measurements. *Int. J. Pharm.* **135**:43–52 (1996).